Estuarine, Coastal and Shelf Science 235 (2020) 106615

Contents lists available at ScienceDirect

Estuarine, Coastal and Shelf Science

journal homepage: http://www.elsevier.com/locate/ecss

An estimation method for blue tide distribution in Tokyo Bay based on sulfur concentrations using Geostationary Ocean Color Imager (GOCI)

Hiroto Higa [a,*], Shogo Sugahara [b], Salem Ibrahim Salem [c,d], Yoshiyuki Nakamura [a], Takayuki Suzuki [a]

[a] Institute of Urban Innovation, Yokohama National University, Hodogaya, Yokohama, Kanagawa, 240-8501, Japan
[b] Department of Chemistry, Graduate School of Natural Science and Technology, Shimane University, 1060, Nishikawatsu, Matsue, Shimane, 690-8504, Japan
[c] Nagamori Institute of Actuators, Kyoto University of Advanced Science, 18 Yamanouchi, Gotanda, Ukyo, Kyoto, 615-8577, Japan
[d] Faculty of Engineering, Alexandria University, Lotfy El-Sied St. Off Gamal Abd El-Naser-Alexandria, Alexandria, 11432, Egypt

ARTICLE INFO

Keywords:
Ocean color remote sensing
Blue tide
Sulfur
GOCI
Regional index term
Japan
Tokyo bay

ABSTRACT

Blue tide, which occurs in eutrophic semi-enclosed bays, is recognized as an important environmental problem because it causes mass mortality of fish and shellfish. In Tokyo Bay, which is a typical eutrophic semi-enclosed bay in Japan, fishery damage due to blue tide is frequently reported. Continuous monitoring is needed for effective water environment management and conservation because blue tides can be too short in duration to observe in the course of field observations. The aim of this study is to develop a model for estimating the distribution of blue tide based on sulfur concentration, which is a key element associated with blue tide. Using real-time data from the Geostationary Ocean Color Imager (GOCI) to estimate sulfur concentrations, we can clearly identify the spatial distributions of blue tides. We developed an empirical model using *in situ* measurement of sulfur and remote sensing reflectance to obtain sulfur concentration ($R^2 = 0.851$). The developed model was applied to GOCI images acquired shortly after field observations during a blue tide on 24 August 2015 in Tokyo Bay in order to validate the accuracy of the sulfur estimation. Estimated and measured sulfur concentration showed less difference when the time between the start of field observations and GOCI image capture was comparatively small ($R^2 = 0.704$). Further, the blue tide distributions could be estimated by applying the developed model to other images acquired during blue tide occurrences at other dates and years. In conclusion, spatial distributions of blue tide in Tokyo Bay can be adequately estimated based on sulfur concentration determined from GOCI images.

1. Introduction

Occurrences of blue tide have been reported in semi-enclosed water areas with high levels of organic pollution and anoxic bottom waters (Suzuki, 2001; Takahashi et al., 2009; Furukawa, 2015; Tomita et al., 2016). Blue tides occur when bottom water containing sulfide (H_2S) generated by anaerobic bacteria rises to the surface in an upwelling phenomenon due to external forces such as continuous winds. When H_2S from the upwelling reacts with oxygen, sulfur colloid particles are generated, and light scattering of sulfur colloid particles results in significant blue coloration at the ocean surface, producing a phenomenon called blue tide. Tokyo Bay located in southern Kanto, Japan has a temperate humid climate. It is a semi-enclosed environment and highly eutrophic bay. The bay had approximately 50 red tide occurrences (algal blooms) per year and approximately 3 blue tide occurrences per year (Furukawa, 2015). During blue tide occurrences, the upwelling of anoxic water containing H_2S pushes sulfur toward land, resulting in mass mortality of fish and shellfish as the blue tidewater moves into mud flats or shallow waters. Hence, it is regarded as a critical environmental problem.

Many aspects of the dynamics of blue tide, which change dramatically over short time scales, remain unresolved because it is exceedingly difficult to capture the actual state of blue tide occurrences through field observations. In previous studies, dynamics of blue tide and hypoxic conditions, including sulfide concentration and distribution, have been captured through monitoring by sampling from ship expeditions and monitoring by water quality sensors on buoys (Sasaki et al., 2009; Horie et al., 2011; Tanaka et al., 2015). Several numerical simulations for the

* Corresponding author.
E-mail address: higa-h@ynu.ac.jp (H. Higa).

https://doi.org/10.1016/j.ecss.2020.106615
Received 14 June 2019; Received in revised form 17 December 2019; Accepted 21 January 2020
Available online 25 January 2020

phenomenon of blue tide and upwelling have been undertaken (Sasaki, 2000; Zhu and Isobe, 2012; Zhu et al., 2017), but it remains difficult to ascertain the behavior and prediction of blue tide.

Through improvements in coverage and level of detail achievable, monitoring by satellite remote sensing will provide a better understanding of the extent and status of blue tide distributions. Most previous satellite observations such as Sea-viewing Wide Field-of-view Sensor (SeaWiFS) and Moderate-resolution Imaging Spectroradiometer (MODIS) had insufficient temporal resolution for monitoring blue tide, which occurs and disappears on short timescales. The Geostationary Ocean Color Imager (GOCI), which conducts hourly monitoring around the Korean Peninsula and Japan during the daylight hours and has 500 m spatial resolution, is applicable to monitoring blue tide. GOCI is the first geostationary satellite focused on northeast Asia and can monitor ocean color with 8 bands centered at 412, 443, 490, 555, 660, 680, 745 and 865 nm (Choi et al., 2012).

Using GOCI images, blue tide occurrences were identified for the first time on satellite images around the north side of Tokyo Bay close to the shore (Higa et al., 2015). Blue tide distributions were captured under the assumption that sulfur colloid particles, which are generated in a chemical process, have a strong light scattering property (Takeda et al., 1991; Higa et al., 2015). The relationships between light scattering and sulfur concentrations as well as the accuracy of remote sensing for measuring sulfur concentrations require further research. In the present study, we developed a model based on the empirical relationships between remote sensing reflectance (R_{rs}) from GOCI images and sulfur concentration at each sampling location to map blue tide occurrences.

Consequently, the aim of this study is to detect the spatial distributions of blue tide in Tokyo Bay using GOCI images based on the developed model.

2. Methods

2.1. Study site and field data

Tokyo Bay is located in the center of Japan between latitudes 35.00 °N and 35.40 °N and longitudes 139.40 °E and 140.05 °E and is 50 km in the north-south direction and 10–30 km in the east-west direction with an area of 960 km^2 (Fig. 2). Water depth in the bay is relatively shallow, averaging about 15 m. The semi-enclosed shape of the bay means that seawater exchange is gradual; the volume of the bay is 15.0 km^3, inflow from rivers is 8–12 $\times$ 10^9 t/year, and retention time in the bay is about 1.5 months. The bay is eutrophic and has been affected by red tides up to 70 times per year. In the summer season, vertical mixing is restricted by stratification, causing the bottom water to become hypoxic and anoxic when oxygen is consumed by the decomposition of large amounts of organic matter. Blue tide has occurred a maximum of approximately 10 times per year (Furukawa, 2015) when H_2S from the bottom sediments moves into the anoxic bottom water followed by subsequent upwelling of bottom water, as shown in Fig. 1.

Fig. 1. Large blue tide offshore of Makuhari in Tokyo Bay on 24 August 2015. (For interpretation of the references to color in this figure legend, the reader is referred to the Web version of this article.)

Periodic observations at fixed sampling points were conducted by ship between June 2010 and September 2013, as shown in Table 1 and Fig. 2. Chlorophyll-a (Chl-a), total suspended solids (TSS), organic suspended solids (OSS) and inorganic suspended solids (ISS) concentrations were measured at each station. In addition, during a massive blue tide, sulfur concentration was determined for samples collected by ship at 16 stations on 24 August 2015 (Table 2). In addition, continuous monitoring data were collected starting from April 2010 using a multiple water quality sensor (YSI Nanotech, Inc. 6600V2-4M), anemometer (Climatic, Inc. CYG-5106), thermometer (Climatic, Inc. C-HPT) and current meter (YSI Nanotech, Inc. ARGONAUT-XR) installed at the Chiba Wave Observation Tower (Fig. 2), which is managed by the Ministry of Land, Infrastructure and Transport, Regional Development Bureau, Chiba Harbor Office.

Chl-a concentrations were determined by the fluorescence method. Water samples (20 mL) were filtered on 25 mm glass microfiber filters. The filters were immediately immersed in 6 mL of N,N-dimethylformamide (DMF) and stored in the dark at 4 °C for 4 h to extract chlorophyll pigments. Then, a fluorescence spectrophotometer (Turner Designs10-AU-005-CE) was used to measure the chlorophyll fluorescence at 665 nm resulting from excitation at 436 nm, and the emission intensities were converted to Chl-a concentrations (Holm--Hansen et al., 1965; Suzuki and Ishimaru, 1990). Total suspended solids (TSS), organic suspended solids (OSS), and inorganic suspended solids (ISS) were determined gravimetrically (American Public Health Association, 2005). Table 3 summarizes the descriptive statistics of water quality parameters.

During blue tide occurrence, a multiple water quality sensor (JFE Advantech AAQ-176 RINKO) was depth calibrated to 0 m at the water surface and then was lowered down at 0.1–0.2 m per 1 s to the maximum water depth at the 16 stations shown in Table 2. Measurement parameters included depth, temperature, salinity, conductivity, electrical conductivity (EC_{25}), density, sigma-t, Chl-a, turbidity, pH, dissolved oxygen and light quantum.

Water samples (250 mL) for sulfur analysis were filtered on 47 mm glass microfiber filters (Whatman glass microfiber filters Grade GF/F: 0.7 μm). Trapped sulfur on the filter was extracted by new method (unpublished results) and sulfur was analyzed by a method of Bartlett and Skoog (1954). Briefly, the filtered water sample was reacted with 5 mL of sodium hydroxide, 20 mL of n-hexane and 15 mL of sodium cyanide (NaCN) in 95% acetone solution for the cyanolysis reaction. After 30 min, ferric chloride ($FeCl_3$) in 95% acetone solution was added to color, and the absorbance at 465 nm was measured on a spectrophotometer (Spectrophotometer name), and the sulfur concentration was quantified.

Radiometric measurements were conducted using hyperspectral radiometers (TriOS RAMSES-ARC and ACC). The remote sensing reflectance (R_{rs}) in the field was calculated as

$$R_{rs}(\lambda) = L_w(\lambda) / E_d(0^+, \lambda) \quad (1)$$

where $L_w(\lambda)$ is the radiance leaving the water and $E_d(0+, \lambda)$ is the downwelling irradiance above the sea surface. $L_w(\lambda)$ was determined by the method of Lubac and Loisel (2007). $E_d(0^+, \lambda)$ was measured from deck measurements because in-water measurement just below the sea surface was strongly affected by focusing and defocusing of sunlight by waves at the sea surface.

2.2. Processing of GOCI images

A total of 18 GOCI images taken over the study area were used. Twelve images corresponding to dates of periodic observation from

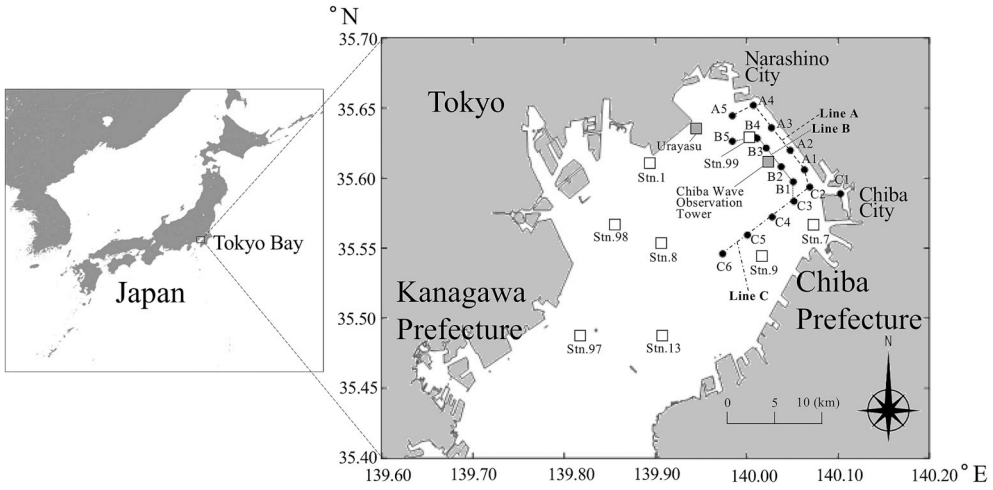

Fig. 2. Location of Tokyo Bay and locations of sampling stations in Tokyo Bay. Solid circles represent stations where *in situ* radiometric measurements, water quality vertical profiles, and water samples were collected on 24 August 2015. Open squares represent stations where *in situ* radiometric measurements and water quality profiles were conducted in 18 surveys between June 2010 and August 2013. Gray squares indicate the locations of the Urayasu and the Chiba Wave Observation Tower where water quality was measured at the surface, middle and bottom layers starting from April 2010 by the Ministry of Land, Infrastructure, Transport and Tourism, Kanto Regional Development Bureau.

Table 1
Periodic observations (date and location) conducted from 2010 to 2013 in Tokyo Bay.

Station ID (coordinates)	Sampling Date	Station ID (coordinates)	Sampling Date
(35.629°N 140.009°E)	2010/09/01 2010/10/04 2011/05/23 2011/06/22 2011/07/26 2011/08/30 2011/09/27 2011/10/24 2012/05/01 2012/06/12 2012/08/07 2012/10/10 2012/12/18 2013/05/08 2013/07/10	(35.566°N 139.856°E)	2010/08/10 2010/10/04 2011/05/23 2011/06/22 2011/08/30 2011/09/27 2011/10/24 2012/05/01 2012/06/12 2012/08/07 2012/10/10 2012/12/18 2013/05/08 2013/07/10 2013/08/08
8 (35.554°N 139.907°E)	2010/06/07 2010/08/10 2010/09/01 2010/10/04 2011/05/23 2011/06/22 2011/07/26 2011/08/30 2011/09/27 2011/10/24 2012/05/01 2012/06/12 2012/08/07 2012/10/10 2012/12/18 2013/05/08 2013/07/10 2013/08/08	13 (35.488°N 139.907°E)	2010/06/07 2010/08/10 2010/10/04 2011/05/23 2011/06/22 2011/08/30 2011/09/27 2011/10/24 2012/05/01 2012/08/07 2012/10/10 2012/12/18 2013/05/08 2013/07/10 2013/08/08
97 (35.488°N 139.819°E)	2011/08/30 2011/09/27 2011/10/24 2012/05/01 2012/06/12 2012/08/07	9 (35.540°N 140.019°E)	2011/10/24
1 (35.612°N 139.895°E)	2011/08/30 2011/09/27 2011/10/24	7 (35.565°N 140.073°E)	2011/09/27

Table 2
In situ sulfur values on 24 August 2015 at each sampling location during a massive blue tide occurrence.

Time	Station ID	Latitude (°N)	Longitude (°E)	Sulfur (mgS/l)
2015/8/24 16:33	A1	35.606	140.063	0.6
2015/8/24 16:52	A2	35.620	140.048	0.7
2015/8/24 17:11	A3	35.636	140.027	0.6
2015/8/24 17:31	A4	35.652	140.007	0.7
2015/8/24 9:04	A5	35.645	139.985	0.4
2015/8/24 12:48	B1	35.597	140.051	0.3
2015/8/24 12:21	B2	35.608	140.037	0.5
2015/8/24 11:57	B3	35.622	140.021	0.4
2015/8/24 11:12	B4	35.628	140.012	0.6
2015/8/24 10:20	B5	35.626	139.984	missing data
2015/8/24 15:56	C1	35.589	140.103	0.8
2015/8/24 15:06	C2	35.594	140.069	0.8
2015/8/24 14:48	C3	35.584	140.051	missing data
2015/8/24 14:32	C4	35.572	140.028	missing data
2015/8/24 13:50	C5	35.560	140.001	missing data
2015/8/24 13:22	C6	35.546	139.973	missing data

Table 3
Descriptive statistics of the water quality parameters measured in periodic observations (N = 77).

Parameter	Minimum	Maximum	Mean	Median	Standard deviation
Chl-a (μg/l)	0.8	102.1	27.4	16.1	26.2
TSS (mg/l)	3.0	26.3	8.3	8.0	3.8
OSS (mg/l)	0.5	17.2	3.8	3.2	2.6
ISS (mg/l)	0.3	12.3	4.7	4.5	2.4

2010 to 2013 were acquired for the R_{rs} calibration with radiometric measurement. Clear images (without cloud cover) on dates corresponding to periodic observation were acquired on 22 June 2011, 30 August 2011 and 8 May 2013, and images at 9:30, 10:30, 11:30 or 12:30, which is close to the sampling time between about 9:00 and 12:30 were used. During the blue tide occurrence on 24 August 2015 (same day as *in*

situ measurements), one image was acquired at 13:30 (7 other images taken that day had cloud cover and were not selected). Eight additional images acquired during blue tide occurrences between 2010 and 2014 as identified from annual reports of the Chiba Prefectural Environmental Research Center were used.

Atmospheric correction of the GOCI images was executed by the MUMM atmospheric correction method developed by Ruddick et al. (2000) using SeaDAS (version 7.3.2) on a 64 bit Linux machine. The MUMM atmospheric correction, which is often applied to highly turbid water (Fettweis, Nechad, & Van den Eynde, 2007; Kowalczuk et al., 2010; Choi et al., 2014), is applicable to our target blue tide in order to account for the effects of high light scattering.

3. Results

3.1. Water quality during blue tide occurrence

A blue tide occurrence in Tokyo Bay was observed from 24 to 27 August 2015. Blue tide tends to occur in the part of Tokyo Bay along Lines A and B (Fig. 2) close to land. Sampling Line C is set along the Chiba navigation channel where H_2S readily accumulates.

Patterns in physical and chemical parameters at the Chiba Wave Observation Tower from 20 to 28 August 2015 show changes preceding the development of blue tide (Fig. 3). A south wind changed to a north wind from 23 August, and the surface current vector flowed in the same direction as the north wind from 23 August at 13:00. In contrast, the current vector at the bottom layer changed to be opposite of the direction at the surface causing bottom water to upwell to the surface. The water temperature at all layers was relatively high, which decreased after the blue tide occurrence. Salinity in all layers increased until 27 August at 6:00, and the bottom water was in a condition of hypoxia or anoxia where the DO in all the layers was decreasing during this time. Turbidity increased in all layers due to increased light scattering of sulfur particles, which were generated in the reaction of sulfide with oxygen during the upwelling.

Fig. 4 shows the linear space interpolation of temperature, salinity, DO and turbidity for the averaged values at the surface (0 m) to 1 m at each station along Lines A, B and C for measurements taken on 24 August 2015. As shown in Fig. 4 (a) and (b), the bottom water upwelled and spread over the surface as a water mass of low temperature and high salinity appeared along the north side of the bay. As shown in the DO interpolation in Fig. 4 (c), the upwelled water was anoxic and hypoxic, but DO increased farther offshore due to dilution of upwelled water as it spread from land to offshore. In particular, hypoxic and anoxic water, which has a DO below 1.0 mg/l, was focused toward the side of Chiba Port. The turbidity distribution shown in Fig. 4 (d) shows increasing turbidity along the offshore sides of Chiba Port and Narashino but lower turbidity around the center part of north side of the bay due to the

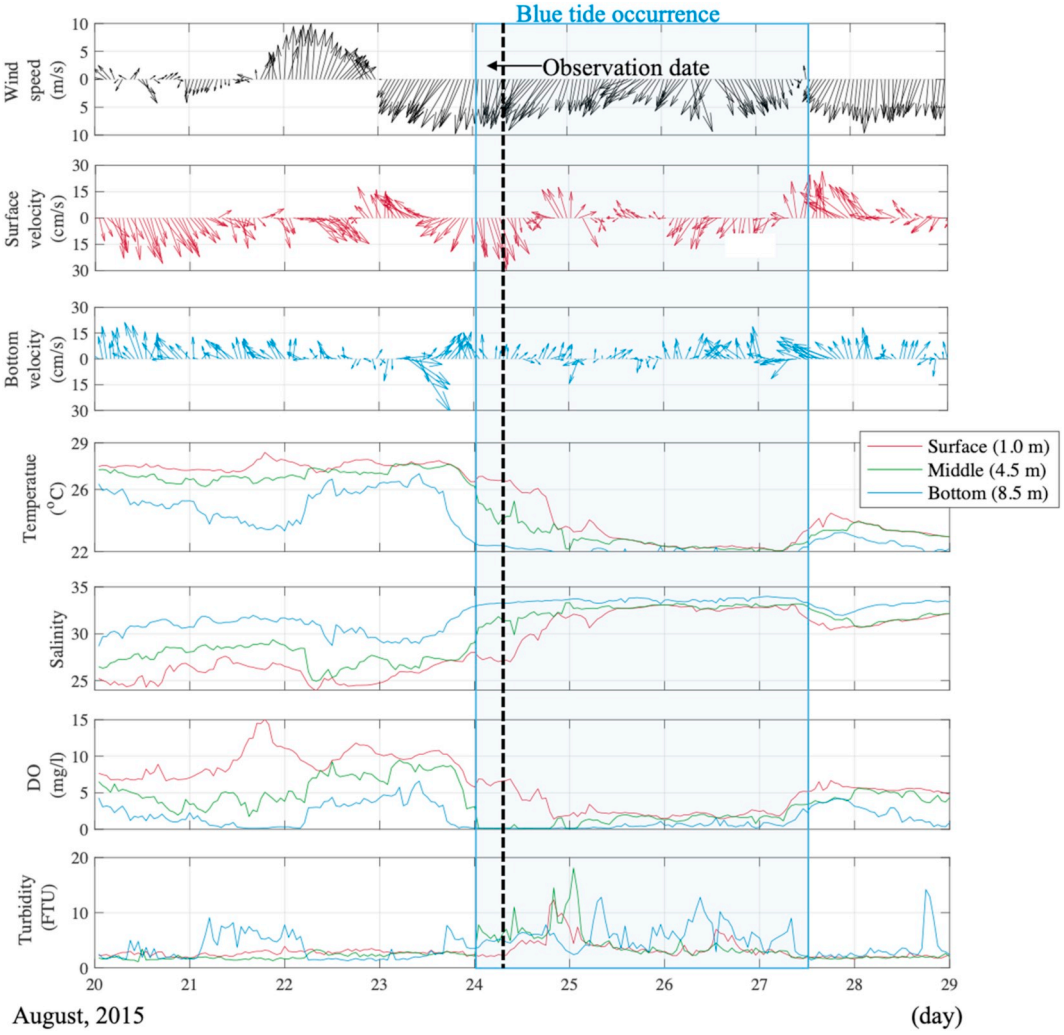

Fig. 3. Physical and chemical parameters at the surface (1.0 m), middle (4.5 m) and bottom layers (8.5 m) obtained by continuous monitoring at the Chiba Wave Observation Tower from 20 to 29 August 2015 covering the period before, during and after the blue tide. (For interpretation of the references to color in this figure legend, the reader is referred to the Web version of this article.)

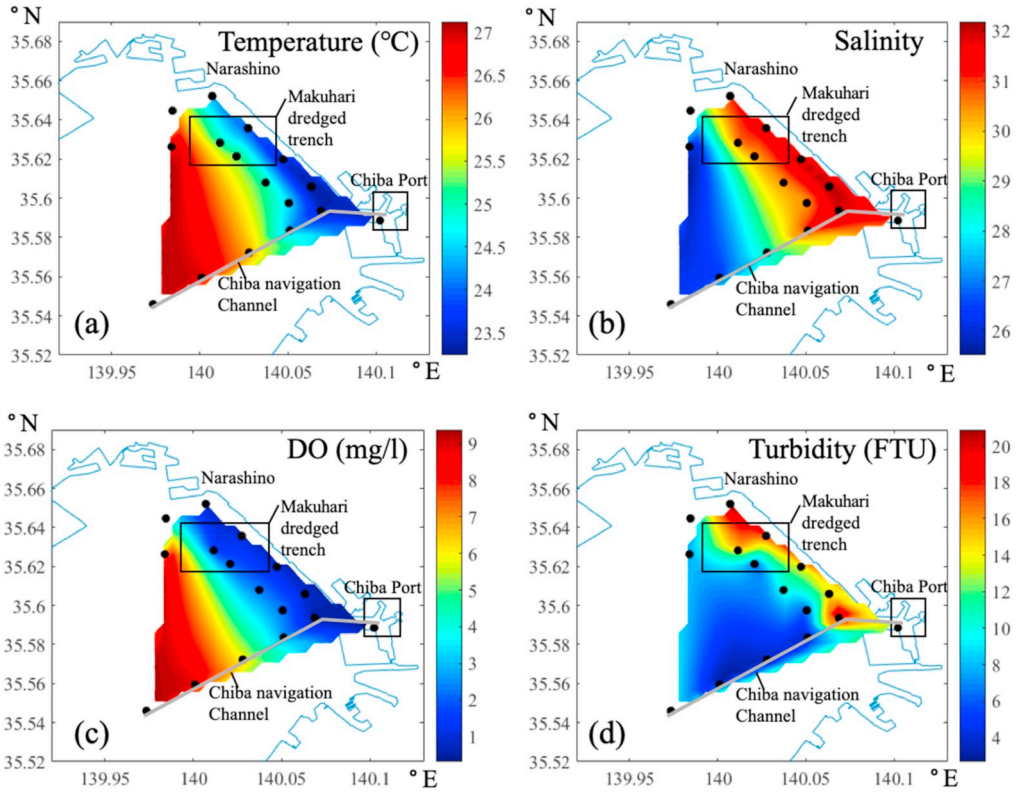

Fig. 4. Spatial distribution of temperature (a), salinity (b), dissolved oxygen (DO) (c) and turbidity (d) measured by ship during a blue tide event. Observations made on 24 August 2015 were used to interpolate average values at 0–1 m at each station. (For interpretation of the references to color in this figure legend, the reader is referred to the Web version of this article.)

turbidity sensors detecting the sulfur colloid particles with high light scattering for the blue tide. Offshore of Chiba Port and Narashino, anoxic water containing high concentrations of upwelled H_2S contributed to an expanded area of high turbidity.

Sampling points at Line A (i.e., from A5 to A1), C2, Line B (i.e., from B5 to B1) and C3 (Fig. 2) were selected to determine the vertical magnitude of blue tide. Fig. 5 shows cross-sections of temperature, salinity, DO and turbidity along Lines A and B. Temperature and salinity

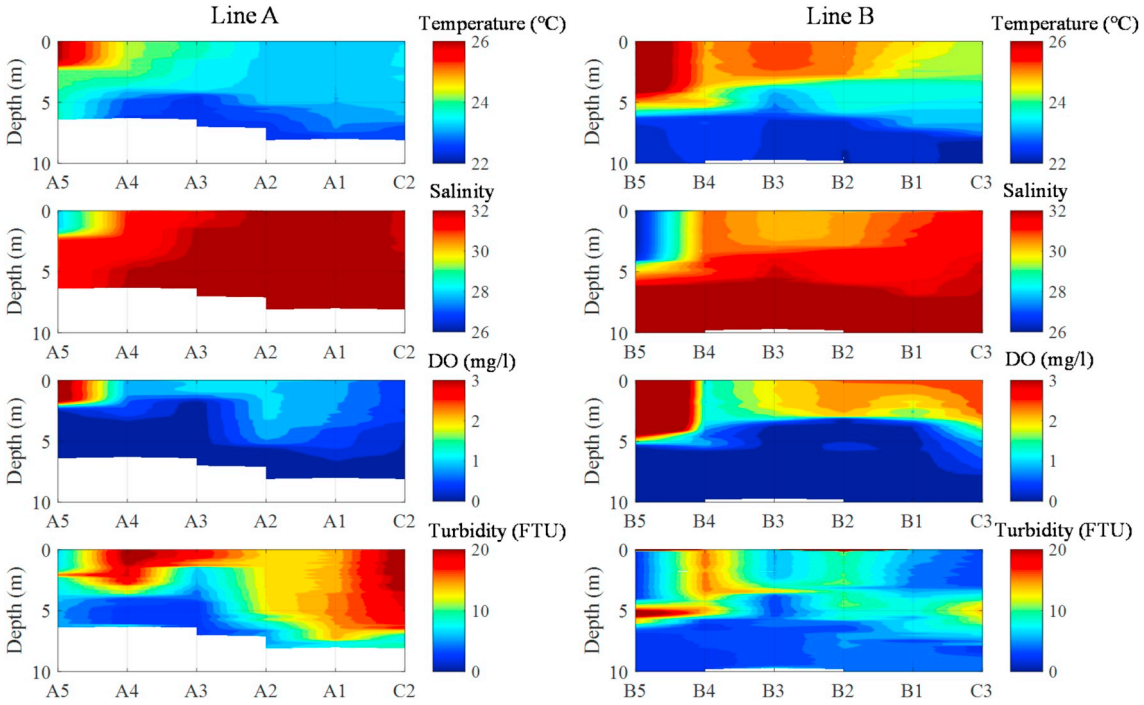

Fig. 5. Vertical profiles of temperature, salinity, dissolved oxygen and turbidity observed on 24 August 2015. Line A and Line B, which are constructed of observation stations A1, A2, A3, A4, A5 and C1, and B1, B2, B3, B4, B5 and C2, respectively.

were mostly vertically uniform from A2 to C2 due to the upwelling of a water mass that causes a drop in water temperature and increase in salinity originated from the bottom layer. DO was below 1.0 mg/l in this region of low temperature and high salinity. Turbidity increased from the bottom to the surface at A1 and C2 around the area offshore of Chiba Port and also increased from around 0 to 5 m at A4. The blue tide at Chiba Port and offshore Narashino was similar in extent vertically and horizontally. Turbidity at A3 increased at around 0–2 m suggesting that the effect of upwelling from Makuhari dredged trench and Chiba navigation channels was small or the blue tide water flowed from A4. Line B, which is on the offshore side of Line A, has larger differences in temperature and salinity between the surface and the bottom, and DO at Line B reached 2.0 mg/l higher at B4 to C3 than at Line A. Further, blue tide water reached to the offshore side of Line B based on increased turbidity around 0–5 m at B2 and B4. Thus, the upwelling bottom water extended from the land side of Line A to the offshore side of Line B, while mixing and upwelling water containing sulfur colloid particles expanded over the area while maintaining high sulfur concentration, particularly at the two stations of B2 and B4.

As described in the background, the blue tide is a phenomenon in which H_2S contained in anoxic water at the bottom upwells due to external forces such as wind and oxidizes in the surface layer to generate sulfur that causes a change in the ocean color to be blue-white color. Hence, the presence of sulfur in the surface water by a series of processes included in the upwelling phenomenon means that the blue tide has occurred. From the observation measurements in Figs. 3–5, it is clear that the upwelling of the bottom water occurred, and the turbidity increased in the region where DO concentration was low. Spatially, turbidity increases at the stations of A1, A2, A3, A4, A5, B1, B2, B3, B4, C1, and C2 in Figs. 4 and 5, and it can be confirmed that *in situ* sulfur concentrations were detected at these stations as shown in Table 2. From the fact that the upwelling phenomenon and sulfur concentrations were detected from the field observations, it can be concluded that the blue tide clearly started on August 24. In addition, the presence of the sulfur colloid particles, which are the origin of blue tides, significantly increased the scattering characteristics. The presence of sulfur colloid particles was detected by the turbidity sensor of infrared backscattering (LED) used in this study. As a result, we proposed turbidity estimation models to estimate sulfur concentrations using ocean color remote sensing. However, since the knowledge about the influence of sulfur concentrations on R_{rs} is unknown, we investigated the relationship between them in the next section with the following outline. Firstly, the measured R_{rs} during the occurrence of the blue tide and the non-blue tide were compared to determine the optical characteristics when sulfur concentration increases. Furthermore, the appropriate wavelengths for estimation of sulfur concentrations will be determined by investigating the relationship between R_{rs} and sulfur concentrations measured during the occurrence of the blue tide and the non-blue tide. Finally, the estimation of sulfur concentration will be conducted by applying a turbidity estimation method.

3.2. Sulfur estimation model

Radiometric measurements at each station on Lines A, B and C and during periodic observation show a peak R_{rs} of 570 nm during the blue tide and much higher R_{rs} between 400 and 700 nm than around wavelengths shorter than 400 nm and longer than 700 nm (Fig. 6). In addition, R_{rs} at the blue light region of wavelengths was likely decreased due to the light absorption effect of CDOM and detritus, which is present in the bottom water. The R_{rs} from blue tide observations was around 5 to 8 times higher than that from periodic observations from 2010 to 2013 (N = 77; black lines in Fig. 6). Although the characteristics of light absorption and light scattering of pure sulfur colloid particles, the cause of blue tides, are not known for sure at the present moment and it has to elucidate in the future, it was confirmed that sulfur colloid particles have clearly strong light scattering properties in visible and infrared

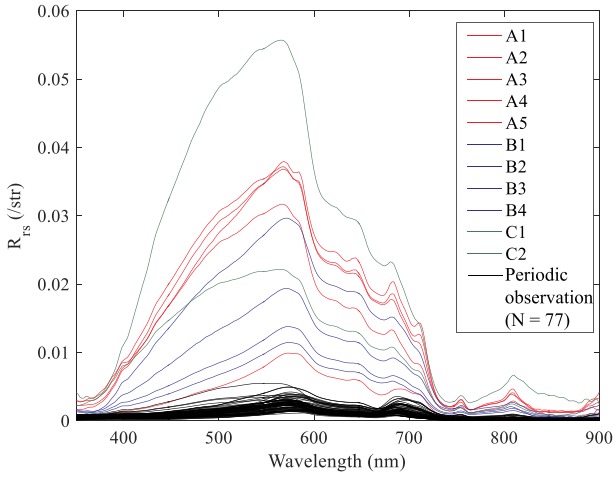

Fig. 6. Reflectance spectra acquired in Tokyo Bay. The red, blue and green reflectance spectra acquired at Line A, Line B and Line C during the blue tide occurrence on 24 August 2015. Reflectance spectra acquired during periodic observation from 2010 to 2013 are shown as black lines. (For interpretation of the references to color in this figure legend, the reader is referred to the Web version of this article.)

wavelengths. Hence, light scattering of sulfur colloid particles in blue tide can be detected by turbidity sensors, as shown in Figs. 3–5.

Many researchers reported that turbidity can be monitored in coastal waters using remote sensing data at the red or near infrared band (Nechad et al., 2009; Petus et al., 2010; Dogliotti et al., 2015; Quang et al., 2017). In order to determine the optimal band position for estimating sulfur concentration, it is necessary to differentiate light scattering in the case of both the presence and absence of sulfur. Thus, the data set of 24 August 2015, which was acquired during a blue tide occurrence, was taken as the blue tide data and the data set from the periodic observation from 2010 to 2013 was taken as the baseline optical characteristics of Tokyo Bay without blue tide. Regression analysis between sulfur concentrations and R_{rs} was performed using data from the two datasets and determining the slope and intercept. The optimum wavelength was determined by taking the logarithm of R_{rs} in order to distinguish between light scattering due to sulfur and other factors. The minimum root mean square error (RMSE) was 0.106 mg/l at R_{rs} of 664 nm, and the RMSE for R_{rs} was low from 580 to 670 nm (Fig. 7). Thus, sulfur concentration can be estimated using the red satellite sensor band in a similar manner as the previous turbidity estimation methods based on a single band (Nechad et al., 2009; Petus et al., 2010; Dogliotti et al., 2015; Quang et al., 2017).

The relationship between *in situ* sulfur concentrations and R_{rs} for the different bands of the GOCI is shown in Fig. 8, where $R_{rs}(490)$, $R_{rs}(555)$, $R_{rs}(660)$ and $R_{rs}(680)$ showed a coefficient of determination of more than 0.8 with *in situ* sulfur.

Light scattering of sulfur particles strongly affects the visible wavelength R_{rs}. The regression equation for sulfur estimation using $R_{rs}(660)$, which has the highest coefficient of determination, is described by the following:

$$\text{Sulfur} = 0.752 \times \log_{10}[R_{rs}(660)] + 2.020 \quad (2)$$

In the sulfur estimation model using $R_{rs}(660)$ described in Equation (2), the difference in light scattering is large between the presence and absence of sulfur. Thus, it is possible to separate light scattering due to sulfur from signal from other particles in water. Generally, 660 nm is the light absorption region of phytoplankton, but light absorption by phytoplankton at 660 nm should be small because phytoplankton largely does not exist in blue tide water, which originates from the bottom. Therefore, the 660 nm band is the most useful of the GOCI bands for estimating sulfur. Equation (2) estimates sulfur concentrations based

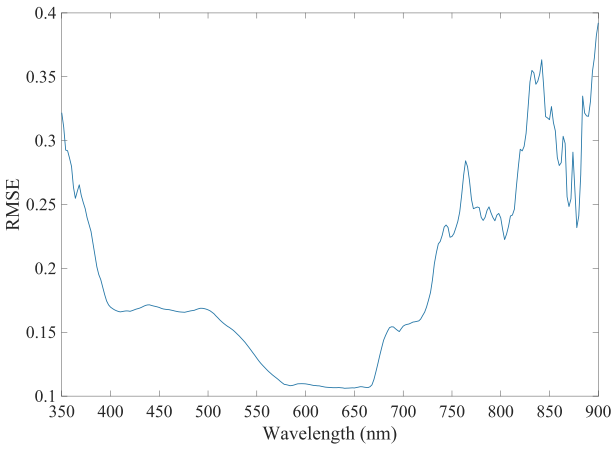

Fig. 7. RMSE of sulfur estimation using a method developed for the *in situ* data set collected during the blue tide on 24 August 2015 and the data set of periodic observations from 2010 to 2013 in order to separate light scattering of sulfur colloid particles in areas with blue tide from waters without blue tide. (For interpretation of the references to color in this figure legend, the reader is referred to the Web version of this article.)

on a single-band turbidity model by determining with or without sulfur using $R_{rs}(660)$. However, a threshold value of $R_{rs}(660)$ was set to 0.00207, and if $R_{rs}(660)$ greater or equal this threshold value, it is judged that sulfur colloid particles exist in the water, and the sulfur concentrations can be estimated by the sulfur model. Therefore, in the study of the sulfur estimation model using the observed data of the current condition, it is confirmed that the existence of sulfur can be appropriately discriminated by the threshold value. But it is erroneously determined when the amount of inorganic suspended matter significantly increases in the estuarine areas. In addition, it is necessary to mask satellite images based on cloud flags because there is concern about the influence of clouds due to the use of the single-band model.

3.3. Mapping blue tide and validation

Blue tides in Tokyo Bay are triggered by north winds producing a surface water current from the inner part of the bay to the Pacific Ocean, which is in the opposite direction as the bottom current. The subsequent upwelling along the coastline of the inner side of the bay results in blue tides occurring at the boundary between the water side and land side of the inner part of the bay. The conditions that produce a north wind during the period from the beginning of summer to fall are low pressure periods and typhoons, in which case, the bay is covered by clouds. Hence, to avoid the effect of cloud cover as much as possible and to capture blue tide distribution, which covers a small area near land, geostationary ocean color satellite GOCI, which has high spatial and temporal resolution, was selected to monitor blue tides.

In order to apply Equation (2), which was developed through field measurements, to GOCI images, we calibrated the *in situ* R_{rs} that was derived from GOCI. Data from 22 June 2011, 30 August 2011, 8 May 2013 and 24 August 2015 were used for the calibration. The relationships between *in situ* R_{rs} based on the center wavelengths of GOCI bands are shown in Fig. 9. The correlation coefficients for each relationship were high (i.e., R^2 more than 0.92) except for at 412, 745 and 865 nm. Note that the equations might have uncertainties because the numbers of the samples for the calibration are not enough. For the sulfur estimation model developed in this study, calibration of R_{rs} at 660 nm is required when using the regression equation. Band calibration was applied to the GOCI image acquired at 13:30 local time on 24 August 2015 during the blue tide occurrence and simultaneous with our field observation, and Equation (2) was applied to the calibrated data, resulting in the image shown in Fig. 10 and the spectrum of the reflectance in Fig. 11.

As shown in the result of Fig. 11, the GOCI R_{rs} spectra have a clearly higher magnitude in the region where the blue tide occurred comparing with non-blue tide spectra. Also, it can be seen that these spectral shapes and magnitudes were similar to *in situ* R_{rs} with the blue tide in Fig. 6. In addition, although there are many gaps in the data due to cloud cover near land, increased sulfur concentration was observed around the north side of the bay in Fig. 10. Since it was impossible to compare *in situ* sulfur

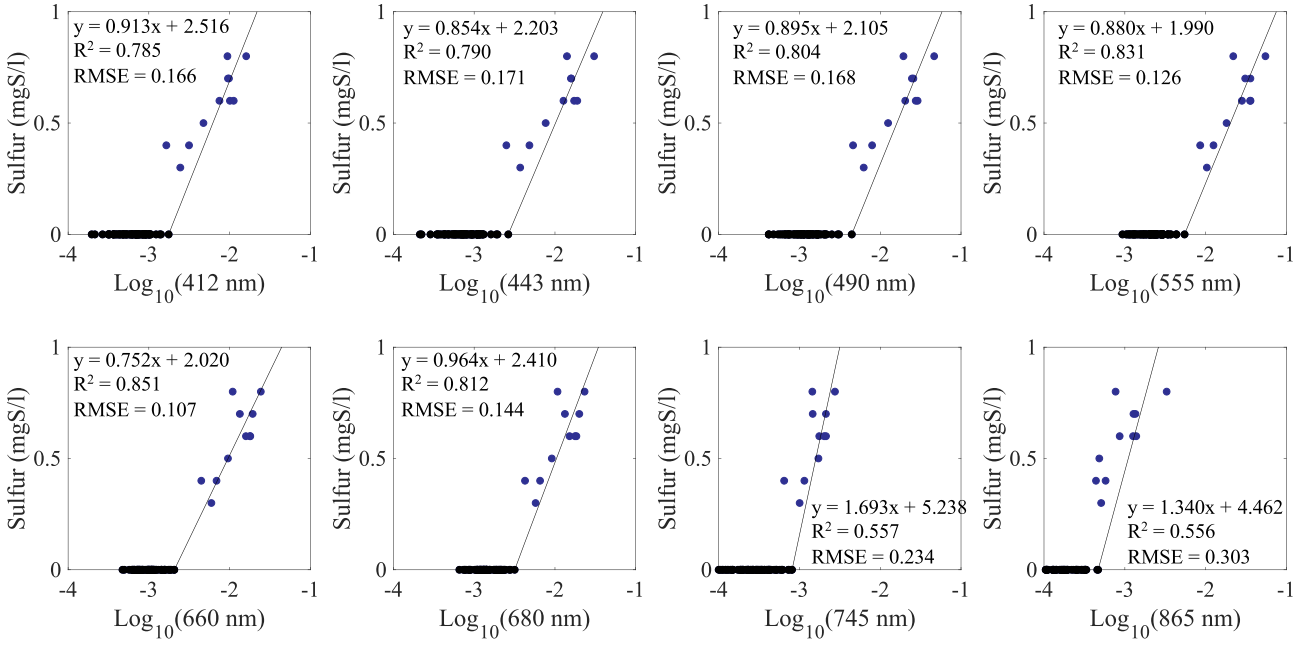

Fig. 8. Relationships between *in situ* sulfur and logarithm of R_{rs} at 412, 443, 490, 555, 660, 680, 745 and 865 nm fixing at a base point of maximum R_{rs} that was acquired on 7 August 2012 when R_{rs} was elevated at Stn. 98 in the estuarine area. The black filled circles represent R_{rs} measured in periodic field observations from 2010 to 2013, blue filled circles represent R_{rs} measured during blue tide on 24 August 2015. (For interpretation of the references to color in this figure legend, the reader is referred to the Web version of this article.)

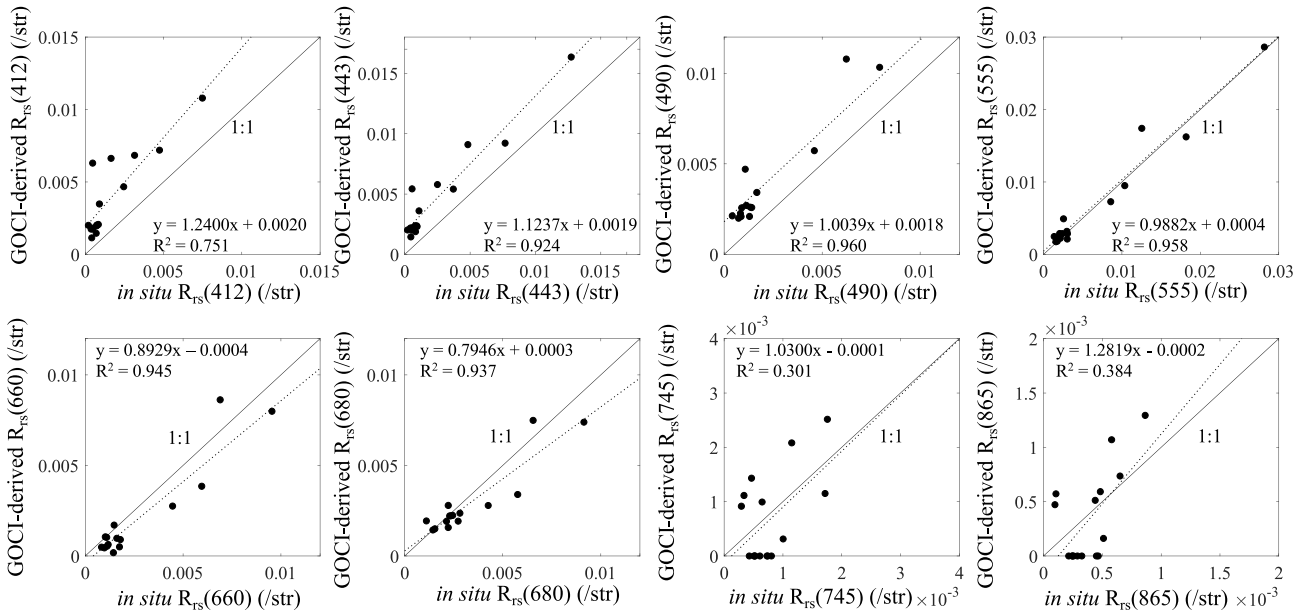

Fig. 9. Comparison at R_{rs}(412), R_{rs}(443), R_{rs}(490), R_{rs}(555), R_{rs}(660), R_{rs}(680), R_{rs}(745) and R_{rs}(865) and *in situ* measurements using 16 samples collected from Tokyo Bay on various dates: 3 samples on 22 June 2011, 5 samples on 30 August 2011, 2 samples on 8 May 2013 and 5 samples on 24 August 2015.

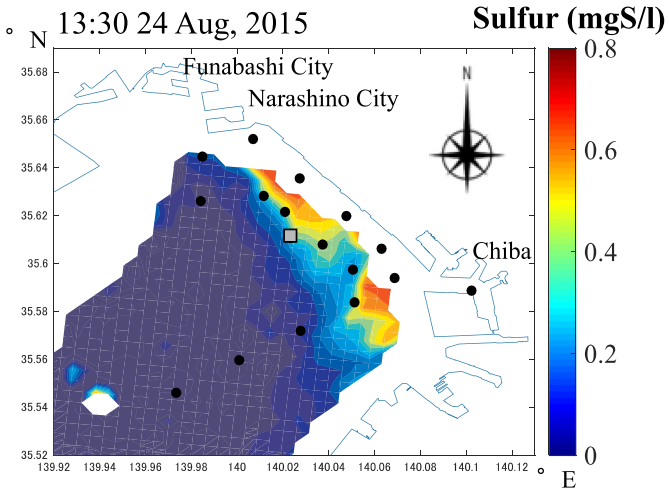

Fig. 10. Estimated blue tide distribution based on applying the sulfur estimation model in Equation (2) to the GOCI image acquired on 24 August 2015 at 13:30. (For interpretation of the references to color in this figure legend, the reader is referred to the Web version of this article.)

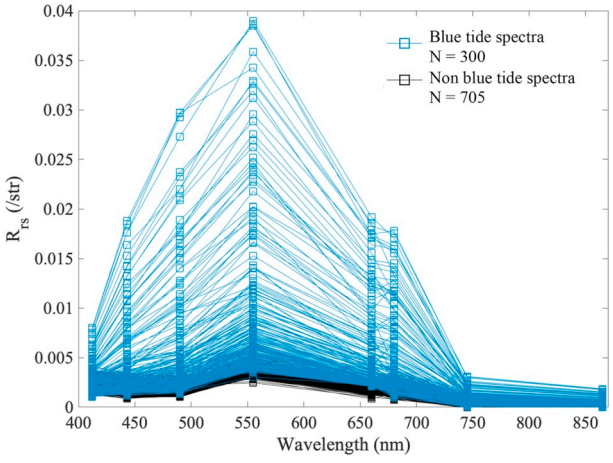

Fig. 11. Reflectance spectra from the GOCI image acquired on 24 August 2015 at 13:30 at Tokyo Bay region shown in Fig. 10. The blue and black reflectance spectra indicate the blue tide and non-blue tide R_{rs}, respectively. (For interpretation of the references to color in this figure legend, the reader is referred to the Web version of this article.)

with estimated sulfur at stations near land, five samples at stations A5, B1, B2, B3, and B4, which were located relatively far offshore, were used for the comparison. The results of the comparison are shown in Fig. 12. The contour colors in Fig. 12 indicate the time difference in the start of field observations and the GOCI image capture time. Based on Fig. 12, sulfur concentration was estimated with high accuracy from stations B1 to B4 with an average time difference of 71.5 min (maximum: 124 min at B4, minimum: 28 min at B1). By comparison, sulfur at A5 was underestimated compared to *in situ* sulfur and the time difference was comparatively large (252 min). This finding suggests that it is possible that the blue tide water had reached A5 at the time when the *in situ* sulfur and R_{rs} were measured, but it went away from A5 at 252 min after the satellite image acquisition time. Based on these findings, it is considered that satellite images capture the spatial distribution of sulfur concentration in real time.

The sulfur estimation model was additionally applied to other GOCI images that were acquired during blue tide occurrences in Tokyo Bay as recorded by the Chiba Prefectural Environmental Research Center. From the June 2010 launch of COMS/GOCI, 6 images, which were acquired on 23 May 2012 at 10:30 and 11:30, on 24 September 2012 at 9:30 and 11:30, and on 2 September 2012 at 13:30 and 14:30, could be applied to the sulfur estimation model developed here (Fig. 13). For all of these images, the estimated sulfur concentrations indicated the locations of blue tides. Continuous monitoring data of wind conditions, temperature, salinity, DO and turbidity around satellite images acquisition time at the Urayasu from 20 to 24 May 2012 (a), at the Chiba Wave Observation Tower from 22 to 25 September 2012 (b), and at the Urayasu from 31 August to 3 September 2014 (c) are shown in Fig. 14. Based on a north wind being observed during all periods with blue tide, a north wind was considered to be a trigger for the occurrence of blue tides. Further, upwelling of bottom water and the occurrence of blue tides were confirmed based on the findings of a decrease in temperature and DO and increase

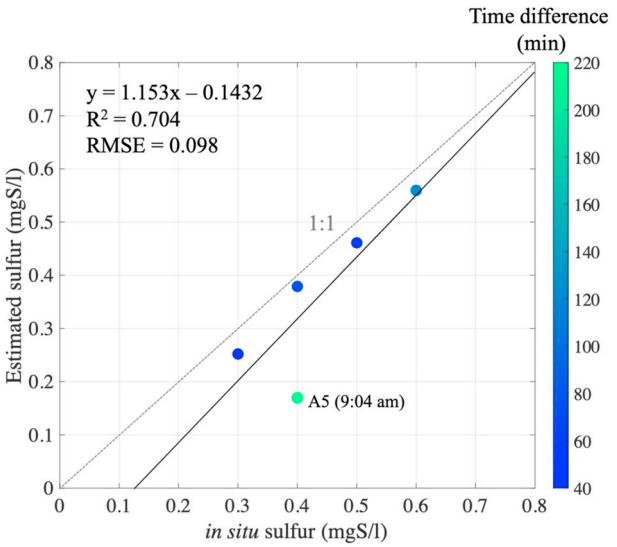

Fig. 12. Scatter plot of sulfur concentration derived from GOCI images acquired on 24 August 2015 at 13:30 using sulfur estimation model in Equation (2) and *in situ* measurement. Color in the scatter plots expresses the time differences between observation time at 9:04, 12:48, 12:21, 11: 57 and 11:12 at A5, B1, B2, B3 and B4, respectively, and the GCOI image acquired at 13:30. (For interpretation of the references to color in this figure legend, the reader is referred to the Web version of this article.)

in salinity and turbidity for all period in Fig. 14. These results suggest that the model developed here may be valid for estimating blue tide distributions based on sulfur concentration.

4. Discussion and conclusion

In this study, field observations were conducted to target a massive blue tide that occurred on 24 August 2015 in order to examine the relationship between R_{rs} and sulfur concentration. The R_{rs} spectrum of the blue tide showed a peak at 570 nm, and it is assumed that the decreasing R_{rs} at the shorter wavelengths around 350–500 nm is due to light absorption effects of CDOM and detritus that originates in the bottom water and might also affect the light absorption of sulfur particles.

In addition, comparing averaged R_{rs} of the blue tide to averaged measurements from periodic observations conducted in the absence of blue tide in Tokyo Bay (N = 77) showed that the intensity of R_{rs} at 660 nm was 5–8 times larger for blue tide. Therefore, it was confirmed that light scattering of sulfur colloid particles was significantly large.

We developed a sulfur estimation model using the logarithm of $R_{rs}(660)$ to set a baseline point based on R_{rs} measured during a blue tide occurrence (N = 11) and the R_{rs} collected during periodic optical observations from 2010 to 2013 (N = 77) based on the light scattering of sulfur colloid particles being significantly larger than in the absence of blue tide. The $R_{rs}(660)$ has been used to estimate suspended solids and turbidity in water in several remote sensing studies (Nechad et al., 2009; Petus et al., 2010; Dogliotti et al., 2015; Quang et al., 2017). The accuracy of turbidity estimation by a simple band model usually decreases due to absorption of light on phytoplankton in the water. However, in the case of blue tide, the water originates in the bottom where phytoplankton is mostly absent, and it is considered that light scattering of sulfur colloid particles can be estimated by $R_{rs}(660)$ as light absorption of phytoplankton from 660 to 670 nm is negligible. In the sulfur estimation model developed here, regarding the separation method for the area with sulfur and the area with no sulfur, the sample, which was obtained on 7 August 2012 when R_{rs} increased at Stn. 98 of the estuarine area, became a base point of the regression line. By using this method, it was basically possible to separate the light scattering of sulfur colloid

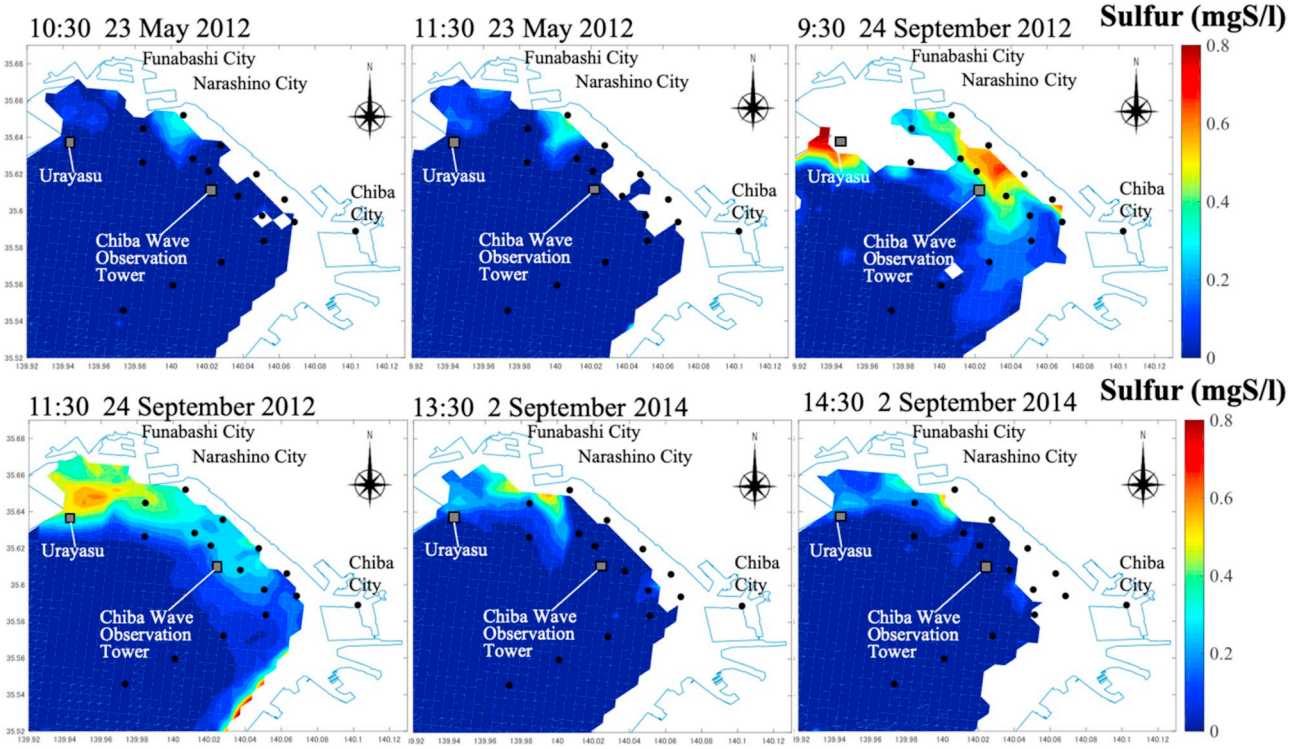

Fig. 13. Maps of sulfur concentration distributions estimated by Equation (2) of the sulfur estimation model. Sulfur maps were obtained from the GOCI acquired at (a) 10:30 local time on 23 May 2012, (b) 11:30 on 23 May 2012, (c) 9:30 on 24 September 2012, (d) 11:30 on 24 September 2012, (e) 13:30 on 2 September 2014 and (f) 14:30 on 2 September 2014.

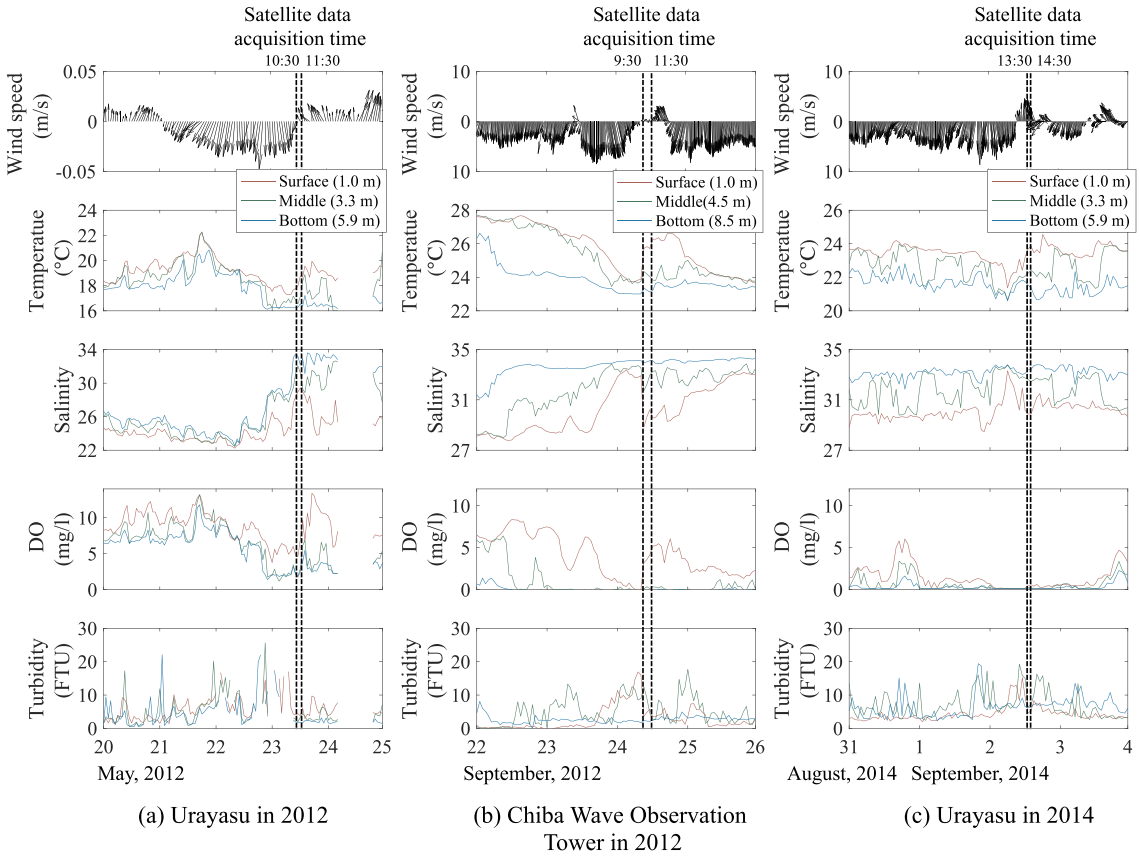

Fig. 14. Physical and chemical parameters obtained by continuous monitoring at the Urayasu from 20 to 24 May 2012 (a), at the Chiba Wave Observation Tower from 22 to 25 September 2012 (b), and at the Urayasu from 31 August to 3 September 2014.

particles from the light scattering of other matter, but the estimation model would be limited by extended periods of heavy rain and large amounts of inorganic matter discharged from rivers into the estuarine area of Tokyo Bay. Therefore, it is necessary to analyze the response of R_{rs} against increases and decreases in inorganic matter and sulfur colloid particles by transfer radiative simulation.

Applying MUMM atmospheric correction and linear regression equations of the band calibration with *in situ* R_{rs} (Fig. 9) to the GOCI image acquired during a massive blue tide showed that the sulfur estimation model is applicable to estimating blue tide distribution. Further, sulfur concentrations can be estimated with high accuracy, which was confirmed by satellite acquisition data collected shortly after sample collection in the field. In this study, the estimation accuracy of sulfur concentration was confirmed by five samples but a larger number of samples is needed for verification of model accuracy. It is difficult to characterize blue tides, which appear and disappear on short time scales, based on field observations done by ship. As shown by the decreased estimation accuracy with a longer gap between field sampling and the satellite acquisition time (Fig. 12), blue tide distributions vary greatly over the time frame of several hours. Therefore, although the number of data points available for confirmation of the method was limited in this study, efforts to accumulate more data by remote sensing and ship observations are expected to refine the predictive capabilities of the remote sensing. At present, it is difficult to distinguish sulfur particles from other particles in backscattering. If it becomes possible to identify differences in optical properties of sulfur particles and other particles, it may be possible to develop a separation algorithm to distinguish them. Moreover, since the estimation model developed in this study is a regression model using *in situ* measurement of sulfur and remote sensing reflectance, it may require re-tuning if used in other regions that suffer from blue tides.

In previous studies, fluctuations in blue tide distributions were deduced based on water temperature, salinity, DO and turbidity values measured at several stations (Sasaki et al., 2009; Horie et al., 2011; Tanaka et al., 2015). In this study, we demonstrated for the first time that the expansion of blue tide could be estimated based on sulfur concentrations by using GOCI images and a sulfur estimation model. This method makes it not only possible to easily monitor blue tide distribution but also to detect blue tide distributions in historical observations. This method can also contribute to elucidating the behavior and verification of numerical simulations for blue tide in Tokyo Bay. From these results, we conclude that GOCI imaging data with sulfur estimation modeling can be used to estimate blue tide dynamics in Tokyo Bay. Future field studies are needed in order to validate the applicability of this method to other water bodies by sampling sulfur *in situ* in various eutrophic water areas where blue tide occurs.

Declaration of competing interest

The authors declare no conflicts of interest associated with this manuscript.

CRediT authorship contribution statement

Hiroto Higa: Conceptualization, Formal analysis, Writing - original draft. **Shogo Sugahara:** Conceptualization, Formal analysis, Writing - original draft. **Salem Ibrahim Salem:** Conceptualization, Formal analysis, Writing - original draft. **Yoshiyuki Nakamura:** Conceptualization, Formal analysis, Writing - original draft. **Takayuki Suzuki:** Conceptualization, Formal analysis, Writing - original draft.

Acknowledgments

This research was a part of the project titled, "Proposals of the Effective Countermeasures Against the Attack of Oxygen Depleted Water Mass and Blue Tide to Tidal Flat and Sea Grass Beds Enclosed by Artificial Coastline" (5–1404) funded by the Ministry of the Environment Government of Japan and the project titled, "Sixth Global Change Observation Mission Research Announcement" funded by the Japan Aerospace Exploration Agency (JAXA). In addition, field observations were conducted with the support of Chiba Prefectural Environmental Research Center.

References

American Public Health Association, 2005. Standard Methods for the Examination of Water and Wastewater, vol 54. American Public Health Association, Washington, DC, USA.

Bartlett, J.K., Skoog, D.A., 1954. Colorimetric determination of elemental sulfur in hydrocarbons. Anal. Chem. 26 (6), 1008–1011.

Chiba Prefectural Environmental Research Center. Annual report: Blue Tide Occurrence Situation of Tokyo Bay. https://www.pref.chiba.lg.jp/wit/suishitsu/report/index.html.

Choi, J.K., Park, Y.J., Ahn, J.H., Lim, H.S., Eom, J., Ryu, J.H., 2012. GOCI, the world's first geostationary ocean color observation satellite, for the monitoring of temporal variability in coastal water turbidity. J. Geophys. Res.: Oceans 117 (C9).

Choi, J.K., Park, Y.J., Lee, B.R., Eom, J., Moon, J.E., Ryu, J.H., 2014. Application of the Geostationary Ocean Color Imager (GOCI) to mapping the temporal dynamics of coastal water turbidity. Remote Sens. Environ. 146, 24–35.

Dogliotti, A.I., Ruddick, K.G., Nechad, B., Doxaran, D., Knaeps, E., 2015. A single algorithm to retrieve turbidity from remotely-sensed data in all coastal and estuarine waters. Remote Sens. Environ. 156, 157–168.

Fettweis, M., Nechad, B., Van den Eynde, D., 2007. An estimate of the suspended particulate matter (SPM) transport in the southern North Sea using SeaWiFS images, *in situ* measurements and numerical model results. Continent. Shelf Res. 27 (10–11), 1568–1583.

Furukawa, K., 2015. Eutrophication in Tokyo bay. In: Eutrophication and Oligotrophication in Japanese Estuaries. Springer, Dordrecht, pp. 5–37.

Horie, T., Furukawa, K., Okada, T., 2011. Spatial distribution of hypoxic water mass based on a monitoring campaign of bay environment at Tokyo Bay, Japan. Coastal Engineering Proceedings (32), 1–10. Shanghai, China.

Holm-Hansen, O., Lorenzen, C.J., Holms, R.W., Strickland, J.D.H., 1965. Fluorometric determination of chlorophyll. ICES (Int. Counc. Explor. Sea) J. Mar. Sci. 30 (1), 3–15.

Higa, H., Koibuchi, Y., Kobayashi, H., Toratani, M., Sakuno, Y., 2015. Numerical simulation and remote sensing for the analysis of blue tide distribution in Tokyo Bay in September 2012. J. Adv. Simulat. Sci. Eng. 2 (1), 1–15.

Kowalczuk, P., Darecki, M., Zablocka, M., Gorecka, I., 2010. Validation of empirical and semi-analytical remote sensing algorithms for estimating absorption by coloured dissolved organic matter in the Baltic Sea from SeaWiFS and MODIS imagery. Oceanologia 52 (2), 171–196.

Lubac, B., Loisel, H., 2007. Variability and classification of remote sensing reflectance spectra in the eastern English Channel and southern North Sea. Remote Sens. Environ. 110 (1), 45–58.

Nechad, B., Ruddick, K.G., Neukermans, G., 2009. Calibration and validation of a generic multisensor algorithm for mapping of turbidity in coastal waters. In: Remote Sensing of the Ocean, Sea Ice, and Large Water Regions 2009, Proc. Of Society of Photo-Optical Instrumentation Engineers (SPIE), vol 7473, p. 74730H.

Petus, C., Chust, G., Gohin, F., Doxaran, D., Froidefond, J.M., Sagarminaga, Y., 2010. Estimating turbidity and total suspended matter in the Adour River plume (South Bay of Biscay) using MODIS 250-m imagery. Continent. Shelf Res. 30 (5), 379–392.

Quang, N., Sasaki, J., Higa, H., Huan, N., 2017. Spatiotemporal variation of turbidity based on landsat 8 OLI in cam ranh bay and thuy trieu lagoon. Vietnam. Water 9 (8), 570.

Ruddick, K.G., Ovidio, F., Rijkeboer, M., 2000. Atmospheric correction of seawifs imagery for turbid coastal and inland waters. Appl. Optic. 39, 897–912.

Sasaki, J., 2000. Development of a long-term predictive model for baroclinic circulation and its application to blue tide phenomenon in Tokyo Bay. In: Proc. 27th Int. Conf. On Coastal Eng., vol 4. ASCE, pp. 3870–3883, 2000.

Sasaki, J., Kawamoto, S., Yoshimoto, Y., Ishii, M., Kakino, J., 2009. Evaluation of the amount of hydrogen sulfide in a dredged trench of Tokyo Bay. J. Coast Res. 890–894.

Suzuki, R., Ishimaru, T., 1990. An improved method for the determination of phytoplankton chlorophyll using N, N-dimethylformamide. J. Oceanogr. Soc. Jpn. 46 (4), 190–194.

Suzuki, T., 2001. Oxygen-deficient waters along the Japanese coast and their effects upon the estuarine ecosystem. J. Environ. Qual. 30 (2), 291–302.

Takahashi, T., Nakata, H., Hirano, K., Matsuoka, K., Iwataki, M., Yamaguchi, H., Kasuya, T., 2009. Upwelling of oxygen-depleted water (sumishio) in Omura bay, Japan. J. Oceanogr. 65 (1), 113–120.

Takeda, S., Nimura, Y., Hirano, R., 1991. Optical, biological, and chemical properties of Aoshio, hypoxic milky blue-green water, observed at the head of Tokyo Bay. J. Oceanogr. Soc. Jpn. 47 (4), 126–137.

Tanaka, Y., Nakamura, Y., Ito, H., Tanaka, Y., Yamamoto, S., Suzuki, T., 2015. Field observations at quaysides and coastal area for blue tide event in the inner part of Tokyo Bay. J. Japan Soc. Civ. Eng. Ser. B2 (Coast. Eng.) 71 (2), I_1273–I_1278 (In Japanese with English abstract).

Tomita, A., Nakura, Y., Ishikawa, T., 2016. New direction for environmental water management. Mar. Pollut. Bull. 102 (2), 323–328.

Zhu, Z., Isobe, M., 2012. Criteria for the occurrence of wind-driven coastal upwelling associated with "Aoshio" on the southeast shore of Tokyo Bay. J. Oceanogr. 68 (4), 561–574.

Zhu, Z., Bai, X., Dou, J., Hei, P., 2017. Applying a simple analytical solution to modelling wind-driven coastal upwelling of two-layered fluid at the head of Tokyo bay, Japan. Water 9 (10), 744.